Molecular origin of high free energy barriers for alkali metal ion transfer through ionic liquid–graphene electrode interfaces

Vladislav Ivaništšev,[a] Trinidad Méndez-Morales,[b] Ruth M. Lynden-Bell,[c] Óscar Cabeza,[d] Luis J. Gallego,[b] Luis M. Varela,[b] Maxim V. Fedorov*[e]

In this work we study mechanisms of solvent-mediated ion interactions with charged surfaces in ionic liquids by molecular dynamics simulations, in an attempt to reveal the main trends that determine ion–electrode interactions in ionic liquids. We compare the interfacial behaviour of Li^+ and K^+ at a charged graphene sheet in a room temperature ionic liquid, 1-butyl-3-methylimidazolium tetrafluoroborate, and its mixtures with lithium and potassium tetrafluoroborate salts. Our results show that there are dense interfacial solvation structures in these electrolytes that lead to a formation of high free energy barriers for these alkali metal cations between the bulk and direct contact with the negatively charged surface. We show that the stronger solvation of Li^+ in the ionic liquid leads to the formation of significantly higher interfacial free energy barriers for Li^+ than for K^+. The high free energy barriers observed in our simulations can explain the generally high interfacial resistance in electrochemical storage devices that use ionic liquid-based electrolytes. Overcoming of these barriers is the rate-limiting step in the interfacial transport of alkali metal ions and, hence, appears to be a major drawback for a generalised application of ionic liquids in electrochemistry. Some plausible strategies for future theoretical and experimental work for tuning them are suggested.

Introduction

The Solutions of metal ions in room-temperature ionic liquids (ILs) are an important class of novel electrolytes for applications in electrochemical energy storage, electrodeposition and catalysis.[1–7] IL solutions of alkali metal ions (Li^+ at the first instance) are of particular interest for the development of high energy and power density batteries.[8–11] These are needed for efficient energy storage for intermittent power generation.[6] However, despite the very intensive research in this area there is still a set of open questions related to the non-trivial interfacial behaviour of ILs[12] and mechanisms of ion solvation in ILs.[13,14] Indeed, it has been shown that interfacial behaviour of ions in the Electrical Double Layer (EDL) determines some properties of IL-based electrochemical systems,[15–20] such as their interfacial resistance.[8,21,22] Also, ILs are known to form long-range correlated interfacial structures (solvation layers) at charged surfaces,[12,23–30] and the role of these structures in mechanisms of dissolved ion interactions with the electrodes has not been entirely understood yet.[31]

It has been shown that the processes of Li^+ preferential solvation in the bulk of an electrolyte and its desolvation at the electrolyte–electrode interface make overall significant effect on interfacial and interphasal processes[§] at negatively charged electrodes in Li-ion cells with non-aqueous electrolytes.[32–40] Due to its small size and, consequently, large surface charge density, the Li^+-ion is strongly solvated in most commonly used polar solvents[35,38–44] as well as in ILs.[44–48] To make direct contact with a surface, dissolved ions need to break up their solvation shells and the high energy penalty associated with this process for strongly solvated ions like Li^+ makes a considerable contribution to activation barriers for different interfacial processes in electrochemical systems.[33] In a series of works by Xu and co-workers, it has been shown that the activation barriers associated with the interfacial desolvation of Li^+ in polar organic electrolytes can be as high as 40–50 kJ mol^{-1}.[35,38–40]

Ishihara *et al.* recently reported experimental activation energies of lithium ion transfer reactions at the interface between $Li_4Ti_5O_{12}$ and organic electrolytes as well as ILs.[18,49] They found the activation energies for lithium ion transfer at the ILs–$Li_4Ti_5O_{12}$ interface to be ~70 kJ mol^{-1}, that is higher than the activation energies for lithium ion at the interface between $Li_4Ti_5O_{12}$ and conventional organic electrolytes (~60 kJ mol^{-1}).[49] These values of the activation energies in ILs reported by Ishihara *et al.* correlate with experimental values of activation energies of Li^+ transport through a solid electrolyte interphase in different IL–electrode systems that vary from 70 to 80 kJ mol^{-1}.[50,51] Interestingly, in the work of Ishihara *et al.* the activation energies for different ILs were reported to be almost the same, regardless of the ion composition of a particular IL.[18]

Ishihara *et al.* attribute the large values of the activation energies to the formation of multilayered structures at the IL–electrode interface.[18] This hypothesis is supported by the results of several recent molecular modelling studies,[52–55] where it was shown that the formation of interfacial solvation layers at a charged surface in IL can lead to high free-energy barriers for dissolved ions to come into a direct contact with the electrode surface. It has been suggested that the formation of these high free-energy barriers is due to a competition between the IL ions and the dissolved ions for the favourable electrostatic interactions with the surface.[53–55] Indeed, even in the case of favourable electrostatic interactions between a counter-ion and the electrode, there is a significant energy penalty for passing the dense interfacial solvation structure and partial desorption of IL ions from the point of contact between the ion and the surface.[53,54]

Overall, our analysis of the published experimental and theoretical/modelling data on the subject discussed above led us to a conclusion that there are several processes that contribute to formation of the free energy barriers for dissolved metal ions to come into direct contact with negatively charged elec-

trodes in ILs. For an IL-based electrochemical system with a flat non-polarisable electrode that is impenetrable for ions, these processes can be roughly classified into three main categories:

1. Penetration through the dense solvation structures at the IL–electrode interface and the consequent restructuring of the interfacial solvation layers near the point of the ion–electrode contact.
2. Desorption of IL ions from the point of contact between the ion and the electrode surface.
3. Desolvation of the metal ion (release of IL anions from its solvation shell) at the electrode surface.

In this work, we use fully atomistic molecular dynamics simulations to reveal molecular scale details of solute alkali metal ion–electrode interactions in ILs with a focus on the interfacial free energy barriers. To understand the role of ion solvation in the formation of the interfacial free energy barriers we compare behaviour of Li^+ and K^+ at a negatively charged graphene surface in pure 1-butyl-3-methylimidazolium tetrafluoroborate, [BMIm][BF_4], and its mixtures with Li[BF_4] and K[BF_4] salts. It is known that the addition of Li^+ has an effect on interfacial solvation structures in ILs.[19,55,56] To the best of our knowledge, the interfacial behaviour of K + has not been studied but is important for the emerging K-ion electrochemical energy storage technologies. Recent work on carbon electrodes for K-ion batteries demonstrates that rechargeable K-ion batteries might be an alternative to widely used Li-ion batteries.[57] Accordingly, in order to provide a better rationalization of the interfacial behaviour of Li^+ and K^+ ions as well as to show the effect of the cation size on free energy barriers we studied the ion–electrode interactions at different mole fractions of alkali metal salts by means of analysing potentials of mean force (PMFs) as a function of the distance between a probe metal ion and the electrode (z), i.e. the free energy profiles ($\Delta A_{ij}(z)$). Graphene was chosen as the electrode material because of (i) its atomically flat surface and, hence, the possibility to use it as a tentative model to study fundamentals of IL interactions with surfaces[25,58,59] as well as to verify theoretical/modelling results,[52–55] and (ii) overall high interest to IL–graphene systems for electrochemical applications.[59–67]

Technical Details

The systems studied consisted in total of 300 [BMIm][BF_4], Li[BF_4] or K[BF_4] ionic pairs, and two rigid graphene slabs each with the area of 3.408 nm × 3.4433 nm separated by adjustable distance, e.g. 8.5 nm for [BMIm][BF_4]. All simulations of the systems were carried out using the Gromacs 4.6 software[68,69] in an *NVT* ensemble with a temperature of 350 K maintained with a V-rescale thermostat.[70] Ions were packed into the simulation cell with Packmol[71] and using the density values obtained in isobaric-isothermal simulations of every system. At the same time, a single probe ion (Li^+ or K^+) was introduced at different distances from the electrode (z from 0.15 to 2.9 nm in steps of 0.05 nm) in order to generate a series of configurations along the z coordinate perpendicular to the surface, and the number of anions was increased by one to achieve the overall charge neutrality of the simulation cell. Thereafter each system was pre-equilibrated (dt = 0.1 fs for 0.1 ns), electrodes charged (dt = 2 fs for 2 ns), annealed at 1000, 900 and 800 K to produce three replicas (dt = 2 fs for 0.3 ns) and simulated with a defined value of the relative dielectric constant of the medium (dt = 1 fs for 1 ns). In the later runs, data on the force acting on the probe ion were collected in order to calculate the free energy profiles (see below). Simulations at two relative dielectric constant (ε_r) values of 1 and 1.6 were performed to make a comparison to alternative preparation and simulation approaches used in our previous works.[54,55] Within the current approach, all simulations were performed using NaRIBaS scripting framework,[72] and with the total duration of more than 1000 ns which is by one and two orders of magnitudes longer than in Refs. 54 and 55, respectively. The more systematic approach allowed us to find free energy minima that were not resolved and apparently cannot be seen with the probability method used in Ref. 55.

In this work, we present results of simulations performed with ε_r = 1.6 and the OPLS-AA force field with atomic charges taken from Ref. 73. The use of relative dielectric constant is equivalent to scaling atomic charges by a factor of 0.79 to account for the high-frequency electronic polarizability. It has a minor effect on the number density distribution of ions as well as on the calculated free energy profiles probably because the electronic polarization leads only to perturbative effects of the Coulomb coupling in what structure and thermodynamics are concerned.

In the runs with charged surfaces, the charges on the carbon sites on the electrode surface were chosen to give surface charge densities of ±1 e nm^{-2} and zero. The left-hand and right-hand surfaces carried equal and opposite charges. Note that 1 e nm^{-2} = 16 μC cm^{-2}. The long-range electrostatic interactions were treated by the particle mesh Ewald method with a correction to give a pseudo-2d condition.[74,75]

Analysis

The free energy profiles were determined from the mean forces on the probe ions at different distances using the methodology described in Refs. 52–54. These were averaged over all three replica runs for a given surface charge at every distance z. The free energy profiles were then determined by integrating the average force with respect to the distance using Simpson's rule. Error bars shown in Figure 2 were calculated from the variance between the replica runs. We emphasize that these measurements are equilibrium measurements and do not contain direct information about the dynamics of barrier crossing.

The measurement of average total densities and number densities of cations and anions as a function of distance from the surface is straightforward. Numbers of ions, total masses and orientations were averaged in bins lying between $z - \delta z/2$ and $z + \delta z/2$, with δz = 0.02 nm. The radial distribution functions (RDF) were calculated using the g_rdf function from the Gromacs analysis toolbox.[76] Spatial distribution functions

around the probe were calculated using a Gromacs analysis tool – g_spatial.[76] Finally, contour plots for the cylindrically averaged charge density distributions were made in the (*R, z*) plane, where $R^2 = x^2 + y^2$. These Cylindrical Density Functions (CDFs) rely on the symmetry of the system and represent cross sections through the 3D spatial distribution functions. A detailed description of the CDFs and their application to slab geometry is provided in Refs. 14 and 54.

Results and Discussion

Ion salvation in the bulk

To characterise the strength of lithium and potassium ions solvation in bulk [BMIm][BF_4] and its mixtures with the alkali metal salts, we calculated the Li^+–BF_4^- and K^+–BF_4^- PMFs $\Delta A(r)$ using the classical formula for particle–particle PMFs in an isotropic liquid solution:[77]

$$\Delta A_{ij}(r) = -k_B T \ln g_{ij}(r), \quad (1)$$

where $g_{ij}(r)$ is the RDF for the ions of type *i* and *j*, k_B is the Boltzmann constant and *T* is the temperature.

The calculated Li^+–BF_4^- and K^+–BF_4^- PMFs for different mole fractions of corresponding salts are shown in Figure 1. This figure also shows Li^+–Li^+ and K^+–K^+ PMFs that help to understand spatial correlations between the ions in their bulk solutions in the IL at finite concentrations.

The particle–particle PMFs can be considered as a solvent averaged free energy surface along the reaction coordinate of an ion exchange reaction.[13,14,78] Therefore, in the spirit of the Samoilov's concept of ion solvation (originally developed for ions in water),[79–81] we characterise the desolvation free energy barriers for a metal cation M^+ solvated by IL anions A^- by an activation energy E_{MA} which can be calculated from the corresponding $\Delta A_{MA}(r)$ as

$$E_{MA} = \Delta A_{MA}(r_{max}) - \Delta A_{MA}(r_{min}), \quad (2)$$

where the r_{max} and r_{min} are the positions of the *highest* positive maximum and the *lowest* negative minimum of the PMF.

Both Li^+ and K^+ are preferentially solvated in [BMIm][BF_4] and its mixtures with the alkali metal salts as reflected in the deep negative first minima on the Li^+–BF_4^- (−9 kJ mol^{-1}) and K^+–BF_4^- (−6 kJ mol^{-1}) PMFs in Figure 1. However, Li^+ is more strongly solvated than K^+ due to its smaller size and, consequently, larger surface charge density that leads to strong electrostatic interactions between Li^+ and IL anions.[55,82] The activation energy for Li^+ in the pure [BMIm][BF_4] is in the range of 15 kJ mol^{-1} (25 mol%) to 19 kJ mol^{-1} (0 mol%), which is significantly higher than the activation energy for K^+ in the pure [BMIm][BF_4] – from 11 kJ mol^{-1} (25 mol%) to 14 kJ mol^{-1} (0 mol%).[§§] For both ions, the activation energy decreases with the increase of the corresponding metal salt mole fraction. We attribute this decrease to the partial screening of the metal cation–BF_4^- electrostatic interactions by other metal cations in the system. Interestingly, the depths of the first minima on the Li^+–BF_4^- and K^+–BF_4^- PMFs do not change much with the change of salt mole fraction; that means that at the distance of direct contact the local interactions between a metal ion and IL anions are not affected by other metal cations in the system.

The PMFs on Figure 1 show large oscillations at short distances that is a result of local charge density waves in the solvation shells of the ions (so-called overscreening effect),[27,83,84] a phenomenon that is common for ions dissolved in polar liquids[77,78,84–87] and ILs.[13,14,82] Due to the large overscreening, the Li^+–Li^+ and K^+–K^+ PMFs show strong correlations between the metal cations dissolved in [BMIm][BF_4] as reflected by the relatively deep negative minima on these PMFs. The positions of the minima correspond to the formation of solvent-separated co-ion pairs,[88] an effect that has been observed before in concentrated solutions of alkali metal ions in ionic liquids and their mixtures with organic solvents.[47,82,89] Due to the strong binding of the BF_4^- anions to the metal cations, they form a dense solvation shell around a dissolved metal cation and the total negative charge of the anion shell overcompensates the positive charge of the solvated ion; as a result, another metal cation is attracted to the anionic solvation shell of its neighbour co-ion.

Ion-Electrode free energy profiles

Figure 2 shows metal ion–electrode PMFs for all the studied electrolytes at the negatively charged graphene surfaces. All these PMFs possess at least two main minima. On each plot the first minimum, from left, corresponds to the direct contact of the ions with the surface at the distances <0.25 nm for Li^+ and <0.35 nm for K^+. The second minimum is located further from the electrode and corresponds to the solvent-separated contact. One obvious observation from this figure is that there are high free energy barriers for both Li^+ and K^+ to come into a direct contact with the negatively charged surface. Also, judging by the *positive* difference between the first and second minima on these PMFs, the most preferential location of the metal cations is not at the direct contact with the surface but rather at the distance of 0.7–1 nm from the surface that more or less coincides with the *second* interfacial layer of the IL.[53–55] However, details are different for these ions. Firstly, for the same mole fraction, the height of the free energy barrier for Li^+ is significantly higher than for K^+. Secondly, the height of the first Li^+–electrode free energy barrier *increases* with the increase of Li^+ mole fraction in the mixture; at the same time, the height of the first K^+–electrode free energy barrier *decreases* with the increase of K^+ mole fraction in the mixture. Thirdly, for the same mole fraction, the values of the activation energy (estimated as the difference between the amplitude of the highest maxima and the lowest minima on the PMFs) obtained for Li^+ (52–62 kJ mol^{-1}) are markedly higher than the activation energies for K^+ (33–53 kJ mol^{-1}).

We note that the calculated values of the activation energy for Li^+ are close to the reported experimental value (47 kJ mol^{-1}) of the activation energy for Li^+ transfer through the interface between 1-hexyl-3-methylimidazolium tetrafluoroborate, [HMIm][BF_4], and lanthanum lithium titanate

electrode.[22] We also note that the activation energies for Li^+ in direct contact with the electrode calculated in our simulations are in the range of experimental activation energies for lithium ion transfer at different IL–electrode *interphases* reported in the literature (70–80 kJ mol^{-1}).[18,50,51]

The 20–30 kJ mol^{-1} difference between these values can be attributed to the experimental phenomena of intercalation of ions, formation of interphases at the electrodes and differences in the structure of IL ions.[33–35,38–40] Another source of the discrepancy between our modelling data for the free energy barriers and the experimental data is the approximate nature of the approach used in this work, *i.e.* classical molecular dynamics simulations with partial point charges. A more accurate description would probably be provided by using *ab initio* molecular dynamics methods,[90] but they are computationally very demanding, especially in the case of the complex systems such as those considered here; work in this area is highly challenging.[65] We also note that simple point charge models such as the one used here have proved extremely useful in modelling liquids[77,85,91–95] Although they can in principle be improved by including terms such as site dipoles, site quadrupoles and atomic polarisabilities,[96–98] they describe the essential physics of the liquid and so give at least qualitative, if not completely quantitative, results at an acceptable cost in computational resources.

With regards to the nature of the interfacial free energy barriers, we note that preferential interactions between the large IL cations and the graphene surface lead to overcharging the negative surface charge density by an excessive positive charge brought there by the IL cations – so-called effect of interfacial overscreening in ILs.[27,53,99–103] As a result, the repulsive interactions between the excessive positive charge in the cationic layer impedes the metal ions from coming into direct contact with the surface. The effect seems to be general for dissolved cationic species in ILs at least of the size of metal ions.[53–55] As ca be seen in Fig. 4, ion size induces significant changes in the solvation of the salt cations near the graphene surface. The weaker solvation of less densely charged K^+ cations by IL anions is probably the main reason for the lower barriers of this cation relative to those of Li^+. Although the electrostatic interaction is probably the dominant term in free energy barrier, dispersion interactions and entropy are also important.

Figure 3 shows the Poisson electrostatic potentials (Δφ) as a function of distance from a negatively charged electrode for various mole fractions of Li^+ and K^+ ions. One can see the oscillations associated with the ion layering, and also notice a remarkably little change in the Δφ(*z*)-profiles as a function of mole fraction. The overscreening is demonstrated by the overshooting of the first potential maximum compared to the bulk value. We note that as the Poisson potentials shown in Figure 3 are constructed for an infinitesimal probe which does not perturb its surroundings while the Li^+ and K^+ ions certainly do so, it is not possible to make a detailed comparison with the free energy curves shown in Figure 2.

Changes of the local solvent structure at the interface

To obtain more detailed insights into the molecular origin of the high free energy barriers, we examined the local solvent structure around the alkali metal ions at different ion distances from the electrode.

Figure 4 shows the PMFs and CDFs for charge distribution around the alkali metal ions in 25 mol% mixtures of corresponding metal salts with [BMIm][BF_4] (qualitatively, the behaviour of PMFs and CDFs for other salt mole fractions is the same). The CDFs were calculated for the ions used as probes in the PMF calculations. The CDFs are shown for different characteristic positions near the electrode surface as illustrated by the corresponding ion–electrode PMFs. Points 1 (Li^+) and 5 (K^+) correspond to the positions of the first ion–electrode PMF minima; points 2 (Li^+) and 6 (K^+) correspond to the positions of the first PMF maxima; points 3 (Li^+) and 7 (K^+) correspond to the position of the second PMF minima; points 4 (Li^+) and 8 (K^+) correspond to the positions of the second PMF maxima.

Comparison of the CDFs for Li^+ and K^+ explain the difference in the height of the interfacial free energy barriers for these ions. Indeed, Li^+ is so strongly solvated by the IL anions that it brings its negatively charged solvation shell to the interfacial IL layer near the electrode. CDF for the point 2 shows that, at the position of the barrier, the Li^+ is still fully solvated by the IL anions and, therefore, the structure of the interfacial layer is significantly perturbed. That means that there are high energy penalties associated with (i) restructuring of the interfacial layer, and (ii) partial desolvation of Li^+ at the position of its direct contact with the negatively charged surface. Both processes consequently lead to the formation of the high free energy barrier for Li^+ to come to the electrode surface.

In turn, analysis of the K^+ CDFs reveals that the mechanisms of penetration of this cation through the IL interfacial layer are different: the CDF for the point 6 shows that K^+ is already partially desolvated at this point and the free energy barrier is mainly due to unfavourable interactions of the K^+ with the first cationic layer of the IL, rather than due to the energy cost for the K^+ desolvation at the interface.

We note that the CDFs for points 1 and 5 show that both alkali metal ions remain still partially solvated by the IL anions even at the positions of their direct contact with the electrode. Consequently, the unfavourable electrostatic interactions between these anions and the negatively charged electrode lead to overall positive values of the PMFs for the first minima. This effect is particularly visible for the Li^+. As one can see from the density distributions of the $BMIm^+$ and BF_4^- ions (Figure 4, bottom), the strong interactions between Li^+ and BF_4^- lead to a considerable concentration of BF_4^- anions in contact with the cathode reflected by a peak on the corresponding density profile around 0.4 nm.

The CDFs and their comparison with the density distributions for the IL ions also explain why the lowest values of the PMFs correspond to the ion positions at the distances far from the interface. These distances (0.7–1 nm) correspond to the region next to the first IL cationic layer. The IL anions in

the solvation shell of the alkali metal ions favourably interact with the excessive positive charge accumulated in the first layer due to the effect of overscreening in ILs.[27]

This phenomenon produces very large decreases of alkali metal ion transport rates at the electrified interface. Indeed, as a first approximation, a simple formula can be used to estimate the average time for ion transport through the electrolyte–electrode interface t_i as[104,105]

$$t_i \propto \tau \exp(E_A/k_BT), \quad (3)$$

where τ is a pre-exponential factor and E_A is the activation energy of ion transport through the interfacial layer. Similarly to Eq. 3, the interfacial resistance R_i of the electrolyte–electrode interface can be estimated as[22,104,105]

$$R_i \propto \rho \exp(E_A/k_BT), \quad (4)$$

where ρ is a pre-exponential factor.

By Eq. 3, at the temperature of the simulations the interfacial free energy barriers obtained would induce an increase of the average time for cation transport close to the interface by 8 to 9 orders of magnitude for Li^+ and 4 to 8 orders of magnitude for K^+. Consequently, by Eq. 4 these barriers would induce similar increase of the interfacial resistance. That gives a flavour of the importance of this phenomenon for ion transport in these dense ionic media, probably the most serious drawback for the IL-based electrolytes.[27,33]

Then, the high interfacial free energy barriers may dramatically reduce the efficiency of the redox reactions in ILs, preventing the effective use of these electrochemically inert solvents. In order to keep them as alternative solvents in high-voltage advanced electrochemical devices, work must be done to reduce the height of these barriers considerably. The task seems to be a realistic one because the experiments by Sagane *et al.* have shown that the interfacial resistance and the interfacial activation energy for Li^+ transfer through the IL–lanthanum lithium titanate interface depend on both cation and anion composition of the IL electrolyte.[22] Also, the results of Seki *et al.* show that performance characteristics of a lithium battery with an IL-based electrolyte can be optimised by varying the lithium salt concentration.[106]

In this sense, this work provides a useful guide for future theoretical and experimental work by demonstrating that it is the specific form of the solvation of ions in ILs what induces the interfacial free energy barriers. Hence, the height of the barriers as well as the difference between free energy difference minima on both sides of the barrier can be tuned by selecting ILs and additives that significantly modify the structure of the polar nano-regions of the electrolyte and the interface without notably reducing electrochemical stability.

Conclusions

The simulation results presented here reveal detailed mechanisms of ion interactions with negatively charged graphene surface in bulk IL and its mixtures with metal salts for two characteristic alkali metal ions, Li^+ and K^+. Our main findings can be summarised as follows:

- Dense interfacial solvation structures in the IL solutions lead to the formation of high free energy barriers for dissolved cations between the bulk and contact with the electrode. The effect is general for dissolved cationic species in ILs (at least of the size of these metal ions), slowing down ion transport in the region close to the electrode. In addition to the effects of the free energy barriers, the transport rate will be affected by the local viscosity
- Strong interactions between Li^+ and IL anions in the Li^+-ion solvation shell significantly increase the height of the free energy barriers compared to K^+ due to the large energy penalty for desolvation of Li^+.
- Both Li^+ and K^+ remain partially solvated by the IL anions even at the point of direct contact with the negatively charged surface. That leads to positive values of the free energy minima that correspond to the direct contact of the ions with the electrode and a shift of the preferential positions of the ions from the electrode surface towards the IL solvent.

Batteries and supercapacitors are important complements to the use of sustainable, but intermittent, sources of power such as wind and waves. Ionic liquids promise to be “green” electrolytes for batteries but often suffer high electrochemical resistance. The high interfacial free energy barriers observed in our simulations can explain this generally high interfacial resistance in electrochemical systems utilising IL-based electrolytes with alkali metal ions.[33] We think that further optimisation of IL-based electrolytes for energy applications can be done by rational *interface-focused* strategies based on a combination of molecular-scale computational and experimental methods.

Acknowledgements

We acknowledge the supercomputing support from the EPSRC funded ARCHIE-WeSt High Performance Computer centre (www.archie-west.ac.uk, EPSRC grant no. EP/K000586/1) and the Galician Supercomputing Centre (CESGA). The financial support of the Estonian Materials Technology Program Project SLOKT12180T, Project of European Structure Funds SLOKT12026T, Estonian Institutional Research Project IUT20-013 and Estonian Centers of Excellence in Science Project: High-technology Materials for Sustainable Development TK117 is highly appreciated. The financial support of the Spanish Ministry of Economy and Innovation MAT2014-57943-C3-1-P and MAT2014-57943-C3-3-P is gratefully acknowledged. Moreover, this work was funded by the Spanish Ministry of Science and Innovation (Grant No. FIS2012-33126) and by the Xunta de Galicia (AGRUP2015/11). All these research projects were partially supported by FEDER. Funding from the European Union (COST Action CM 1206) and by the Galician Network on Ionic Liquids, REGALIs (CN 2014/015) is also acknowledged.

Notes and references

[§] Hereinafter we refer to the term interphase as a complex wide layer that forms from the decomposition products from the electrolyte, and to the term interface as the boundary layer between the electrode and the electrolyte with a thickness of several molecular diameters, i.e. the EDL.

[§§] Note, the systems with a single probe metal ion have a non-zero mole fraction of 1/300, which we round to 0 mol%.

1 S. Z. El Abedin, M. Polleth, S. A. Meiss, J. Janek and F. Endres, *Green Chem*., 2007, **9**, 549–553.
2 M. Armand, F. Endres, D. R. MacFarlane, H. Ohno and B. Scrosati, *Nat. Mater.*, 2009, **8**, 621–629.
3 J. P. Hallett and T. Welton, *Chem. Rev.*, 2011, **111**, 3508–3576.
4 M. Y. Lui, L. Crowhurst, J. P. Hallett, P. A. Hunt, H. Niedermeyer and T. Welton, *Chem. Sci.*, 2011, **2**, 1491–1496.
5 A. P. Abbott, G. Frisch and K. S. Ryder, *Annu. Rev. Mater. Res.*, 2013, **43**, 335–358.
6 D. R. MacFarlane, N. Tachikawa, M. Forsyth, J. M. Pringle, P. C. Howlett, G. D. Elliott, J. H. Davis, M. Watanabe, P. Simon and C. A. Angell, *Energy Environ. Sci.*, 2014, **7**, 232–250.
7 M. D. Bhatt and C. O'Dwyer, *Phys. Chem. Chem. Phys.*, 2015, **17**, 4799– 4844.
8 J. Schaefer, Y. Lu, S. Moganty, P. Agarwal, N. Jayaprakash and L. Archer, *Appl. Nanosci.*, 2012, **2**, 91–109.
9 N. Madria, T. Arunkumar, N. G. Nair, A. Vadapalli, Y.-W. Huang, S. C. Jones and V. P. Reddy, *J. Power Sources*, 2013, **234**, 277–284.
10 D. Monti, E. Jonsson, M. R. Palacın and P. Johansson, *J. Power Sources*, 2014, **245**, 630–636.
11 Y. Matsui, M. Yamagata, S. Murakami, Y. Saito, T. Higashizaki, E. Ishiko, M. Kono and M. Ishikawa, *J. Power Sources*, 2015, **279**, 766–773.
12 R. Hayes, G. G. Warr and R. Atkin, *Chem. Rev.*, 2015, **115**, 6357–6426.
13 R. M. Lynden-Bell, *J. Chem. Phys.*, 2008, **129**, 204503–7.
14 R. M. Lynden-Bell, *Phys. Chem. Chem. Phys.*, 2010, **12**, 1733–1740.
15 A. A. Aal, R. Al-Salman, M. Al-Zoubi, N. Borissenko, F. Endres, O. Höfft, A. Prowald and S. Zein El Abedin, *Electrochim. Acta*, 2011, **56**, 10295–10305.
16 R. Hayes, N. Borisenko, B. Corr, G. B. Webber, F. Endres and R. Atkin, *Chem. Commun.*, 2012, **48**, 10246–10248.
17 M. Yamagata, N. Nishigaki, S. Nishishita, Y. Matsui, T. Sugimoto, M. Kikuta, T. Higashizaki, M. Kono and M. Ishikawa, *Electrochim. Acta*, 2013, **110**, 181–190.
18 Y. Ishihara, K. Miyazaki, T. Fukutsuka and T. Abe, *J. Electrochem. Soc.*, 2014, **161**, A1939–A1942.
19 N. Borisenko, R. Atkin, A. Lahiri, S. Z. E. Abedin and F. Endres, *J. Phys.: Condens. Matter*, 2014, **26**, 284111.
20 R. Atkin, N. Borisenko, M. Dru¨schler, F. Endres, R. Hayes, B. Huber and B. Roling, *J. Mol. Liq.*, 2014, **192**, 44–54.
21 J. P. Zheng, S. S. Moganty, P. C. Goonetilleke, R. E. Baltus and D. Roy, *J. Phys. Chem. C*, 2011, **115**, 7527–7537.
22 F. Sagane, T. Abe and Z. Ogumi, J. *Electrochem. Soc.*, 2012, **159**, A1766– A1769.
23 F. Endres, O. Höfft, N. Borisenko, L. H. Gasparotto, A. Prowald, R. Al-Salman, T. Carstens, R. Atkin, A. Bund and S. Z. El Abedin, *Phys. Chem. Chem. Phys.*, 2010, **12**, 1724–1732.
24 S. Perkin, Phys. *Chem. Chem. Phys.*, 2012, **14**, 5052–5062.
25 H. Zhou, M. Rouha, G. Feng, S. S. Lee, H. Docherty, P. Fenter, P. T. Cummings, P. F. Fulvio, S. Dai, J. McDonough, V. Presser and Y. Gogotsi, *ACS Nano*, 2012, **6**, 9818–9827.
26 A. I. Frolov, K. Kirchner, T. Kirchner and M. V. *Fedorov, Faraday Discuss.*, 2012, **154**, 235–247.
27 M. V. Fedorov and A. A. Kornyshev, *Chem. Rev.*, 2014, **114**, 2978–3036.
28 S. Perkin and M. Salanne, *J. Phys.: Condens. Matter*, 2014, **26**, 280301.
29 A. J. Page, A. Elbourne, R. Stefanovic, M. A. Addicoat, G. G. Warr, K. Vo¨ıtchovsky and R. Atkin, *Nanoscale*, 2014, **6**, 8100–8106.
30 V. Ivanistsev, S. O'Connor and M. V. Fedorov, *Electrochem. Commun.*, 2014, **48**, 61–64.
31 A. A. Kornyshev and R. Qiao, *J. Phys. Chem. C*, 2014, **118**, 18285–18290.
32 T. Abe, F. Sagane, M. Ohtsuka, Y. Iriyama and Z. Ogumi, *J. Electrochem. Soc.*, 2005, **152**, A2151–A2154.
33 K. Xu, *Chem. Rev.*, 2014, **114**, 11503–11618.
34 H. Moon, R. Tatara, T. Mandai, K. Ueno, K. Yoshida, N. Tachikawa, T. Yasuda, K. Dokko and M. Watanabe, *J. Phys. Chem. C*, 2014, **118**, 20246–20256.
35 K. Xu, A. von Wald Cresce and U. Lee, *Langmuir*, 2010, **26**, 11538–11543.
36 B. Scrosati, J. Hassoun and Y.-K. Sun, *Energy Environ. Sci.*, 2011, **4**, 3287–3295.
37 F. Li, T. Zhang and H. Zhou, *Energy Environ. Sci.*, 2013, **6**, 1125–1141.
38 A. von Wald Cresce and K. Xu, Electrochem. *Solid-State Lett.*, 2011, **14**, A154–A156.
39 K. Xu and A. von Wald Cresce, *J. Mater. Research*, 2012, **27**, 2327–2341.
40 A. von Wald Cresce, O. Borodin and K. Xu, *J. Phys. Chem. C*, 2012, **116**, 26111–26117.
41 M. V. Fedotova, *J. Mol. Liq.*, 2011, **164**, 39–43.
42 M. V. Fedotova, *Russ. J. Gen. Chem.*, 2011, **81**, 1417–1423.
43 M. Takeuchi, N. Matubayasi, Y. Kameda, B. Minofar, S.-i. Ishiguro and Y. Umebayashi, *J. Phys. Chem. B*, 2012, **116**, 6476–6487.
44 M. M. Gafurov, S. A. Kirillov, K. S. Rabadanov, M. B. Ataev and D. O. Tretyakov, *J. Struct. Chem.*, 2014, **55**, 67–71.
45 J. C. Lassegues, J. Grondin and D. Talaga, *Phys. Chem. Chem. Phys.*, 2006, **8**, 5629–5632.
46 S. Duluard, J. Grondin, J. L. Bruneel, I. Pianet, A. Grelard, G. Campet, M. H. Delville and J. C. Lassegues, J*. Raman Spectrosc.*, 2008, **39**, 627– 632.
47 Z. Li, O. Borodin, G. D. Smith and D. Bedrov, *J. Phys. Chem. B*, 2015, **119**, 3085–3096.
48 S. Wilken, S. Xiong, J. Scheers, P. Jacobsson and P. Johansson, *J. Power Sources*, 2015, **275**, 935–942.
49 Y. Ishihara, K. Miyazaki, T. Fukutsuka and T. Abe, *ECS Electrochem. Lett.*, 2014, **3**, A83—A85.
50 S. Seki, Y. Ohno, Y. Kobayashi, H. Miyashiro, A. Usami, Y. Mita, H. Tokuda, M. Watanabe, K. Hayamizu, S. Tsuzuki, M. Hattori and N. Terada, *J. Electrochem. Soc.*, 2007, **154**, A173–A177.
51 G. H. Lane, P. M. Bayley, B. R. Clare, A. S. Best, D. R. MacFarlane, M. Forsyth and A. F. Hollenkamp, *J. Phys. Chem. C*, 2010, **114**, 21775– 21785.
52 M. V. Fedorov and R. M. Lynden-Bell, *Phys. Chem. Chem. Phys.*, 2012, **14**, 2552–2556.
53 R. M. Lynden-Bell, A. I. Frolov and M. V. Fedorov, *Phys. Chem. Chem. Phys.*, 2012, **14**, 2693–2701.
54 V. Ivanistsev, M. V. Fedorov and R. M. Lynden-Bell, *J. Phys. Chem. C*, 2014, **118**, 5841–5847.
55 T. Mendez-Morales, J. Carrete, M. Perez-Rodrıguez, O´. Cabeza, L. J. Gallego, R. M. Lynden-Bell and L. M. Varela, *Phys. Chem. Chem. Phys.*, 2014, **16**, 13271–13278.
56 A. Elbourne, S. McDonald, K. Voıchovsky, F. Endres, G. G. Warr and R. Atkin, *ACS Nano*, 2015, **9**, 7608–7620.

57 Z. Jian, W. Luo and X. Ji, *J. Am. Chem. Soc.*, 2015, 137, 11566–11569.
58 S. Xu, S. Xing, S. S. Pei and S. Baldelli, *J. Phys. Chem. B*, 2014, **118**, 5203–5210.
59 E. Uesugi, H. Goto, R. Eguchi, A. Fujiwara and Y. Kubozono, *Sci. Rep.*, 2013, **3**.
60 Z. S. Wu, W. Ren, L. Xu, F. Li and H.-M. Cheng, *ACS Nano*, 2011, **5**, 5463–5471.
61 Q. Zhang, S. Wu, L. Zhang, J. Lu, F. Verproot, Y. Liu, Z. Xing, J. Li and X.-M. Song, *Biosens. Bioelectron.*, 2011, **26**, 2632–2637.
62 P. Simon and Y. Gogotsi, *Acc. Chem. Res.*, 2013, **46**, 1094–1103.
63 W.-Y. Tsai, R. Lin, S. Murali, L. L. Zhang, J. K. McDonough, R. S. Ruoff, P.-L. Taberna, Y. Gogotsi and P. Simon, *Nano Energy,* 2013, **2**, 403–411.
64 P. L. Huang, X. F. Luo, Y. Y. Peng, N.-W. Pu, M. D. Ger, C. H. Yang, T. Y. Wu and J. K. Chang, *Electrochim. Acta*, 2015, **161**, 371–377.
65 Z. E. Hughes and T. R. Walsh, *Nanoscale*, 2015, **7**, 6883–6908.
66 T. Romann, O. Oll, P. Pikma, K. Kirsimae and E. Lust, *J. Power Sources*, 2015, **280**, 606–611.
67 J.-S. Lee, T. Lee, H.-K. Song, J. Cho and B.-S. Kim, *Energy Environ. Sci.*, 2011, **4**, 4148–4154.
68 B. Hess, C. Kutzner, D. van der Spoel and E. Lindahl, *J. Chem. Theory Comput.*, 2008, **4**, 435–447.
69 S. Pronk, S. Pall, R. Schulz, P. Larsson, P. Bjelkmar, R. Apostolov, M. R. Shirts, J. C. Smith, P. M. Kasson, D. v. d. Spoel, B. Hess and E. Lindahl, *Bioinformatics*, 2013, **29**, 845–854.
70 G. Bussi, D. Donadio and M. Parrinello, *J. Chem. Phys.*, 2007, **126**, 014101–7.
71 L. Martınez, R. Andrade, E. G. Birgin and J. M. Martınez, *J. Comput. Chem.*, 2009, **30**, 2157–2164.
72 V. Ivanistsev, K. Kirchner, K. Karu and M. V. Fedorov, NaRIBaS: A scripting framework for computational modelling of Nanomaterials and Room Temperature Ionic Liquids in Bulk and Slab, www.github.com/vladislavivanistsev/NaRIBaS, 2015.
73 S. V. Sambasivarao and O. Acevedo, J*. Chem. Theory Comput.,* 2009, **5**, 1038–1050.
74 D. Frenkel and B. Smit, Understanding molecular simulation, Academic Press, 2002.
75 I. C. Yeh and M. L. Berkowitz, *J. Chem. Phys.,* 1999, **111**, 3155–3162.
76 B. Hess, D. Van Der Spoel, E. Lindahl, and the GROMACS development team, Gromacs Users Manual version 4.6.5, www.gromacs.org, 2013.
77 F. Hirata, Molecular Theory of Solvation, *Kluwer Academic Publishers*, New York, 2003.
78 M. Fedorov, J. Goodman and S. Schumm, *Phys. Chem. Chem. Phys.*, 2007, **9**, 5423–5435.
79 O. Y. Samoilov, *Faraday Discuss.,* 1957, **24**, 141–146.
80 Structure of aqueous electrolyte solutions and the hydration of ions, ed. O. Y. Samoilov, Consultants Bureau, New York, 1965.
81 M. N. Buslaeva and O. Y. Samoilov, The Chemical Physics of Solvation. Part A, *Elsevier*, Amsterdam, 1985, p. 391–414.
82 T. Mendez-Morales, J. Carrete, S. Bouzon-Capelo, M. Perez-Rodrıguez, O. Cabeza, L. J. Gallego and L. M. Varela, *J. Phys. Chem. B*, 2013, **117**, 3207–3220.
83 A. A. Kornyshev, *Electrochim. Acta*, 1981, **26**, 1–20.
84 A. A. Kornyshev, S. Leikin and G. Sutmann, *Electrochim. Acta*, 1997, **42**, 849–865.
85 R. M. Lynden-Bell and J. C. Rasaiah, J*. Chem. Phys.,* 1997, **107**, 1981–1991.
86 L. M. Varela, M. Garcıa and V. Mosquera, *Phys. Rep*., 2003, **382**, 1–111.
87 M. V. Fedorov and A. A. Kornyshev, *Mol. Phys.,* 2007, **105**, 1–16.
88 Y. Marcus and G. Hefter*, Chem. Rev.,* 2006, **106**, 4585–4621.
89 O. Russina, R. Caminiti, T. Mendez-Morales, J. Carrete, O. Cabeza, L. J. Gallego, L. M. Varela and A. Triolo, *J. Mol. Liq.,* 2014, **205**, 16—21.
90 E. Paek, A. J. Pak and G. S. Hwang, *J. Chem. Phys.,* 2015, **142**, 024701–6.
91 J. P. Hansen and I. R. McDonald, Theory of Simple Liquids, 4th ed, Elsevier Academic Press, Amsterdam, The Netherlands, 2000.
92 J. L. Barrat and J. P. Hansen, Basic concepts for simple and complex liquids, Cambridge University Press, New York, 2003.
93 J. N. Canongia Lopes, J. Deschamps and A. A. H. Padua, *J. Phys. Chem. B*, 2004, **108**, 2038–2047.
94 L. Santos, J. N. Canongia Lopes, J. A. P. Coutinho, J. Esperan¸ca, L. R. Gomes, I. M. Marrucho and L. P. N. Rebelo, *J. Am. Chem. Soc.*, 2007, **129**, 284–285.
95 K. Shimizu, M. F. Costa Gomes, A. A. H. Padua, L. P. N. Rebelo and J. N. Canongia Lopes, *Journal of Molecular Structure: THEOCHEM*, 2010, **946**, 70–76.
96 P. E. M. Lopes, B. Roux and A. D. MacKerell, Theor. *Chem. Acc.*, 2009, **124**, 11–28.
97 C. Merlet, B. Rotenberg, P. A. Madden and M. Salanne, *Phys. Chem. Chem. Phys.,* 2013, **15**, 15781–15792.
98 M. Salanne, *Phys. Chem. Chem. Phys.,* 2015, **17**, 14270–14279.
99 M. V. Fedorov, N. Georgi and A. A. Kornyshev, *Electrochem. Commun.*, 2010, **12**, 296–299.
100 N. Georgi, A. A. Kornyshev and M. V. Fedorov, *J. Electroanal. Chem.,* 2010, **649**, 261–267.
101 V. Ivanistsev and M. V. Fedorov, Electrochem. *Soc. Interface*, 2014, **23**, 65–69.
102 M. Sha, Q. Dou, F. Luo, G. Zhu and G. Wu, ACS Appl. *Mater. Interfaces*, 2014, **6**, 12556–12565.
103 V. Ivanistsev, K. Kirchner, T. Kirchner and M. V. Fedorov, *J. Phys.: Condens. Matter*, 2015, **27**, 102101.
104 J. Bockris and A. K. N. Reddy, Modern electrochemistry. 1, Kluwer Academic Publishers, New York, 2nd edn, 2002, vol. 1.
105 J. O. Bockris, A. K. N. Reddy and M. Gamboa-Aldeco, Modern electrochemistry. 2A, Kluwer Academic Publishers, New York, 2nd edn, 2002, vol. 2A.
106 S. Seki, Y. Ohno, Y. Mita, N. Serizawa, K. Takei and H. Miyashiro, *ECS Electrochem. Lett.,* 2012, **1**, A77–A79.

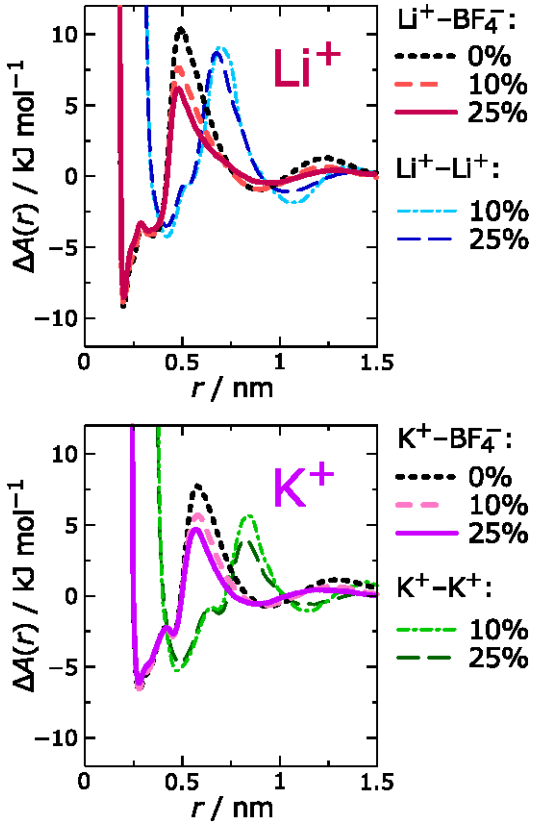

Fig. 1 Calculated Li^+–BF_4^- (TOP) and K^+–BF_4^- (BOTTOM) PMFs for different mole fraction of $Li[BF_4]$ and $K[BF_4]$ salt in $[BMIm][BF_4]$, respectively, as shown on the legend. The figure also shows Li^+–Li^+ (TOP) and K^+–K^+ (BOTTOM) PMFs for 10% and 25% mole fractions to illustrate spatial correlations between the ions in the mixture.

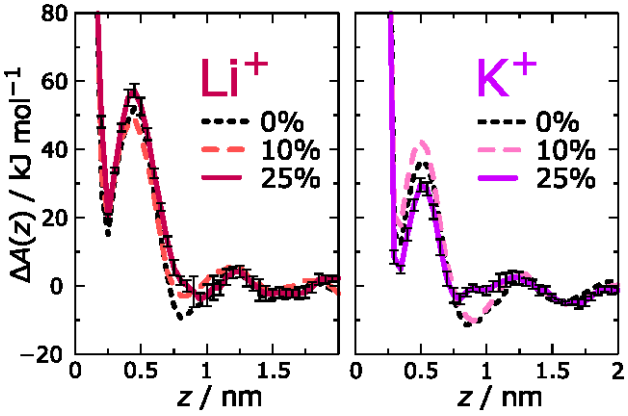

Fig. 2 Alkali metal ion–electrode PMFs for the electrolytes containing Li^+ (LEFT) and K^+ (RIGHT) at the negatively charged graphene surface. The legends indicate the ion mole fraction in $[BMIm][BF_4]$.

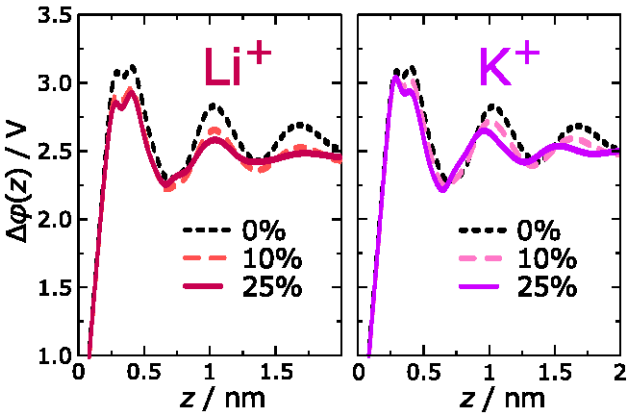

Fig. 3 Poisson electrostatic potentials for the electrolytes containing Li^+ probe (LEFT) and K^+ probe (RIGHT) ions at the negatively charged graphene surface. The legends indicate the ion mole fraction in $[BMIm][BF_4]$.

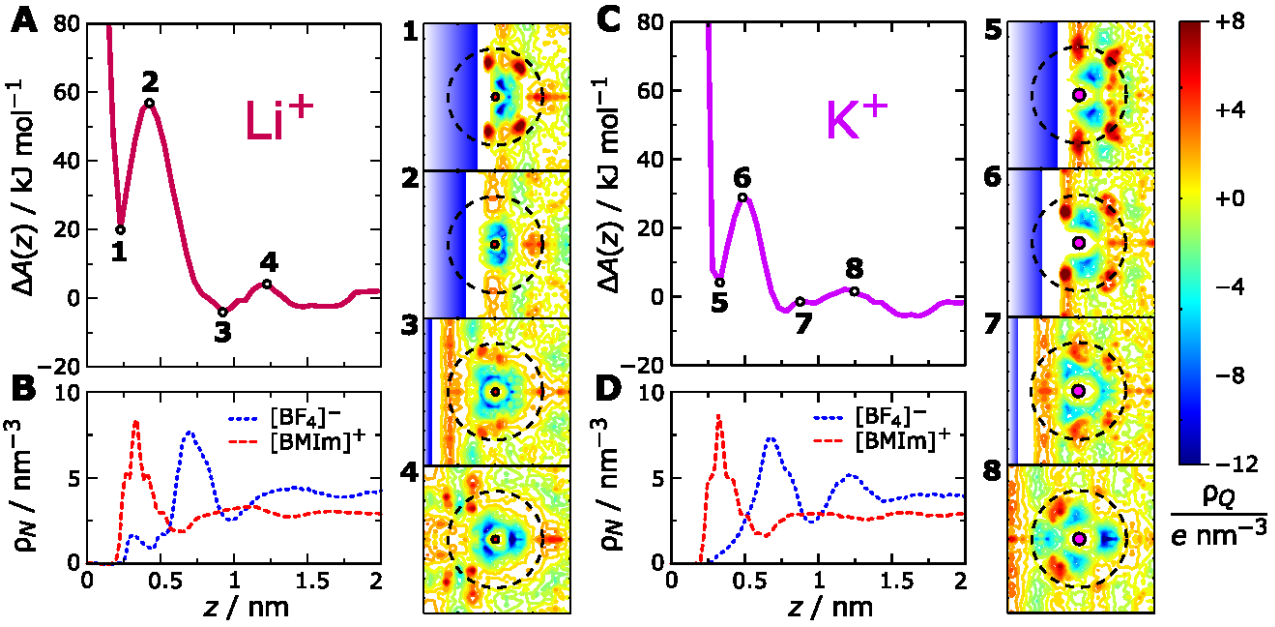

Fig. 4 Alkali metal ion–electrode PMFs (A,C), $BMIm^+$ and BF_4^- number density profiles (B, D) and CDFs for charge distribution around the alkali metal ions in 25 mol% mixtures of corresponding metal salts with $[BMIm][BF_4]$ near the negatively charged graphene surface. The CDFs are shown for different characteristic positions near the electrode surface as illustrated by the corresponding ion–electrode PMFs (A,C).